

Development of Advanced Inductive Scenarios for ITER

T.C. Luce¹, C.D. Challis², S. Ide³, E. Joffrin⁴, Y. Kamada³, P.A. Politzer¹, J. Schweinzer⁵, A.C.C. Sips⁴, J. Stober⁵, G. Giruzzi⁶, C.E. Kessel⁷, M. Murakami⁸, Y.-S. Na⁹, J.M. Park⁸, A.R. Polevoi¹⁰, R.V. Budny⁷, J. Citrin¹¹, J. Garcia⁶, N. Hayashi³, J. Hobirk⁵, B.F. Hudson¹², F. Imbeaux⁶, A. Isayama³, D.C. McDonald², V.V. Parail², T.W. Petrie¹, C.C. Petty¹, T. Suzuki³, M.R. Wade¹, and the ITPA IOS topical group members and experts

¹General Atomics, P.O. Box 85608, San Diego, California 92186-5608, USA

²Euratom/CCFE Fusion Association, Culham Science Centre, Abingdon, OX14 3DB UK

³Japan Atomic Energy Agency, 801-1, Mukouyama, Naka, Ibaraki-ken 311-0193, Japan

⁴JET-EFDA Culham Science Centre, Abingdon, OX14 3DB UK

⁵Max-Planck-Institut für Plasmaphysik, Garching, Germany

⁶CEA, IRFM, 13108 Saint Paul-lez-Durance, France

⁷Princeton Plasma Physics Laboratory, Princeton, New Jersey, USA

⁸Oak Ridge National Laboratory, Oak Ridge, Tennessee 37831, USA

⁹Dept. of Nuclear Engineering, Seoul National U., 599 Gwanangno, Gwanak-Gu, Seoul, 151-744, Korea

¹⁰ITER Organization, Route de Vinon sur Verdon, F-13115 St Paul lez Durance, France

¹¹FOM, Rijnhuizen, the Netherlands

¹²Oak Ridge Associated Universities, Oak Ridge, Tennessee 37831, USA

e-mail contact of main author: luce@fusion.gat.com

Abstract. Since its inception in 2002, the International Tokamak Physics Activity topical group on Integrated Operational Scenarios (IOS) has coordinated experimental and modeling activity on the development of advanced inductive scenarios for applications in the ITER tokamak. This report documents the present status of the physics basis and the prospects for applications in ITER. The key findings of this research activity are: 1) inductive scenarios capable of higher normalized pressure ($\beta_N \geq 2.4$) than the ITER baseline scenario ($\beta_N = 1.8$) with normalized confinement at or above the standard H-mode scaling have been established under stationary conditions on the four largest diverted tokamaks (AUG, DIII-D, JET, JT-60U); 2) the parameter range where high performance is achieved is broad in q_{95} and density (normalized to the empirical density limit); 3) MHD modes can play a key role in reaching stationary high performance, but also define the stability and confinement limits; 4) results from individual machines with unique capabilities for varying rotation, current drive, and heating sources facilitate more realistic projections for ITER performance; 5) coordinated experiments have yielded clearer measurements of the normalized gyroradius scaling that is essential to the projection to ITER; and 6) coordinated modeling activity supports the present research by clarifying the most significant uncertainties in the projections to ITER. Studies extending previous work on pedestal characterization, radiative divertor operation, and edge localized mode suppression to advanced inductive scenarios have also been coordinated through the IOS group.

1. Introduction

Operational scenarios with normalized fusion performance metrics significantly above those envisioned for the ITER baseline scenario (normalized pressure $\beta_N = 1.8$, confinement quality $H_{98y2} = 1$), but still relying on inductive current drive, should play a significant role in ITER. One application is to maximize the neutron fluence per plasma by reducing the plasma current (to save transformer flux for flattop operation) and using the auxiliary current drive systems to provide a significant fraction of the current to extend the duration (limited by the external cooling capacity even for non-inductive scenarios) [1]. Because the optimum current is expected to lie between that of steady-state scenario and the baseline scenario, this type of operation that combines elements of both was called the ITER “hybrid” scenario, and the scenarios discussed here are often referred to by this name. As will be seen later, experiments in present-day tokamaks find stationary inductive discharges with substantially higher β_N than that expected in the baseline scenario. Since the fusion power P_{fus} scales roughly with the square of the pressure p , higher β_N translates directly to higher fluence through higher

fusion power and, to a smaller extent, less flux consumption in flattop through increased conductivity and bootstrap current. However, the combination of higher β_N and good H_{98y2} opens other potential applications. For example, the pressure (and therefore the fusion power) at $q_{95}=4$ is at or above that of the baseline scenario, and the possibility arises of reaching the physics objective of energy gain $Q=10$ at $P_{\text{fus}} = 500$ MW for >400 s at reduced plasma current (11 MA vs 15 MA in the baseline scenario). In the event that the confinement quality in the baseline scenario is less than estimated, these scenarios represent an alternative means to enhance the fusion power while operating at 15 MA, rather than raising the current to 17 MA, which is the present contingency plan. To take into account the broader possibilities of these scenarios for ITER, the term “advanced inductive” scenario, rather than “hybrid” scenario, will be applied here to plasmas with $\beta_N \geq 2.4$ and $H_{98y2} \geq 1$.

Performance metrics to be used here for comparison among present-day tokamak results and projection to ITER include the normalized pressure $\beta_N \equiv \langle p \rangle / \langle B^2 \rangle / (I/aB)$ (pressure normalized to theoretical scaling of the ideal MHD stability limit of a free-boundary plasma) [2], the confinement quality H_{98y2} (thermal energy confinement time normalized to a scaling relation derived from a multi-tokamak database of ELMing H-mode plasmas) [3], the safety factor at the 95% radius q_{95} , the ratio of the density to an empirical density limit $f_{\text{DL}} \equiv n / (I/\pi a^2)$ [4], and a figure of merit related to the energy gain $G \equiv \beta_N H_{89p} / q_{95}^2$ [1], where H_{89p} is the ratio of the global energy confinement to an L-mode scaling [5]. The term “stationary” will be used to describe plasmas with inductive current drive in which the plasma parameters are not changing either on the energy confinement timescale or the global current relaxation timescale $\tau_R \equiv 0.171 R/\mathfrak{R}$, where R is the major radius of the plasma and \mathfrak{R} is the plasma resistance. A more complete discussion of these performance metrics can be found in [1].

The ITPA joint activities have focused on specific questions regarding advanced inductive scenarios. The earliest work focused on establishing the existence domain of the scenarios on the four largest divertor tokamaks (AUG [6], DIII-D [7], JET [8], JT-60U [9]) and looking for common ground in performance and phenomenology. This report will illustrate the commonality of the operational experience. A brief historical perspective is given in [1] and will not be repeated here. Having established a common ground, the joint activities turned to establishing a physics basis for applying these scenarios in ITER. Two key areas have been addressed — the stationary solution to the current profile evolution and projection of the energy confinement. The ITPA group has facilitated both joint experiments and modeling activities in these two areas, and these will be reported briefly here. A summary of the prospects for applying these scenarios in ITER and the key remaining questions will be given.

2. Existence Domains

Stationary plasmas meeting the criteria for an “advanced inductive” scenario have been demonstrated for $>3 \tau_R$ in the four largest divertor tokamaks (AUG, DIII-D, JET, JT-60U). The longest duration plasma (in real time and normalized to τ_R) was achieved in JT-60U (Fig. 1) [9]. A database of plasma parameters from 1095 plasmas from these tokamaks has been compiled for use by the IOS topical group, of which 505 meet the criteria of $\beta_N \geq 2.4$ and $H_{98y2} \geq 1$ for defining advanced inductive operation for durations longer than $5 \tau_E$, which in all cases is a significant fraction of τ_R . This data is a representative, but not exhaustive, sample of the experience in these tokamaks. Figure 2 shows the distribution of the data in current and density, using the dimensionless parameters q_{95} and f_{DL} to facilitate comparison. The range of q_{95} and f_{DL} shown

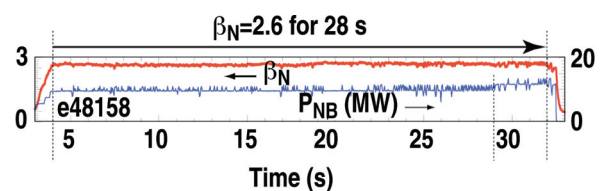


FIG. 1. Longest duration ($>15 \tau_R$) advanced inductive plasma.

Figure 2 shows the distribution of the data in current and density, using the dimensionless parameters q_{95} and f_{DL} to facilitate comparison. The range of q_{95} and f_{DL} shown

represents the region of tokamak operating space of interest for fusion energy. Figure 2 clearly shows that advanced inductive operation has been obtained throughout this domain. Each of the tokamaks has achieved advanced inductive operation across a wide range of q_{95} . The DIII-D and JT-60U data lie primarily at $f_{DL} < 0.5$, while the JET data lie at $f_{DL} > 0.6$. The AUG data span more uniformly the range of f_{DL} , allowing connection to the other tokamaks. It should be noted that the AUG dataset includes data from operations with both carbon and tungsten as the dominant plasma-facing material [10].

Figure 3 shows the achieved β_N versus proxies for the average value of the dimensionless gyroradius, collision frequency, and plasma current. Following Ref. [3], these are defined here as $\rho_* \propto (W_{th}/nV)^{1/2}/Ba$, $\nu^\dagger \propto (n^3V/W_{th}^2)(R^5/a^3)^{1/2}$, and $q_{cyl} \propto BV/IR^2$. Later, a similar proxy of the ratio of the thermal kinetic to magnetic pressure $\beta_{th} \propto W_{th}/VB^2$ will be used. No discernable trend in the achieved β_N with these dimensionless variables can be inferred from this dataset with the exception of the evident correlation of β_N with low ρ_* set by the maximum power or magnetic field available in the tokamak. The maximum β_N is set by the onset of $n=1$ tearing modes in each tokamak [7,11–13]. Because this limit is a resistive mode rather than an ideal mode, the result is often a dramatic loss of energy confinement rather than an immediate disruption. An unmitigated mode can slow the plasma rotation and continue to grow as a non-rotating mode and cause a disruption. However, the relatively slow growth of these modes allows detection and the potential for active means to recover the plasma performance or avoid disruption. At lower pressures, there appear to be systematic trends in the type of MHD

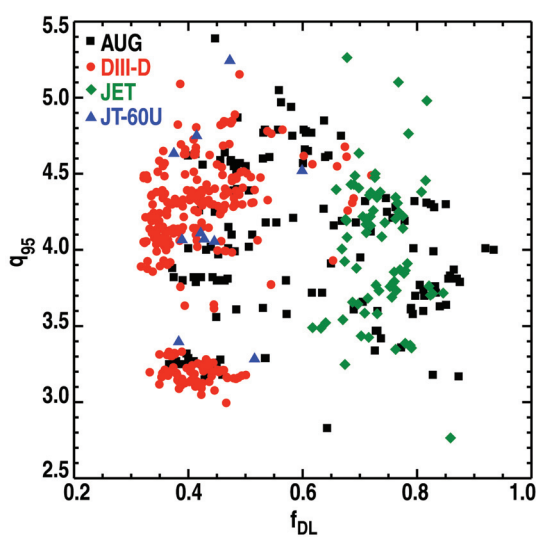


FIG. 2. Distribution of advanced inductive plasmas in the space of normalized plasma current and density.

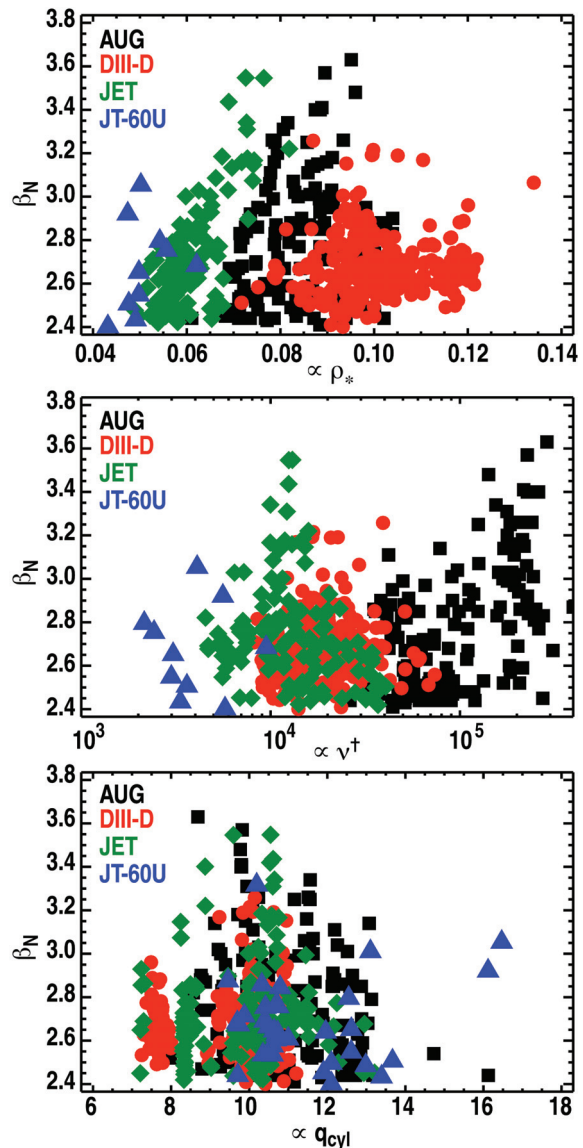


FIG. 3. Achieved β_N vs proxies for dimensionless (a) gyroradius (ITER range is 0.021–0.024 for advanced inductive plasmas), (b) collision frequency (ITER range is 80–170), and (c) plasma current (ITER values are 7.4 and 9.8 for $q_{95}=3$ and 4, respectively) as defined in the text. Symbols and colors as defined in Fig. 2.

observed [8,9,11,14]. Small sawteeth are generally seen for $q_{95} < 4$, but are often absent above this. The disappearance of sawteeth is often correlated with an increase in the operational β_N below the onset of the limiting $n=1$ tearing mode. At higher density, fishbones are frequently observed, while at lower density, $n > 1$ tearing modes appear. The IOS group is working to make a map of the MHD behavior similar to Fig. 2 to quantify the commonality of the phenomena. The impact of MHD in the scenario will be discussed more fully in the next section.

3. Projection to ITER

Two key issues arise in projecting the plasma performance from present-day experiments to ITER. First, the scaling of confinement must be known. Only energy confinement has been studied so far — particle and momentum confinement are also important. Second, both the favorable confinement and stability properties of these scenarios may be tied to the current profile achieved under stationary conditions. The IOS group is working to address both issues with joint experimental and modeling activities.

Figure 4 shows how H_{98y2} varies with the four dimensionless parameter proxies defined above for plasmas with $\beta_N > 2.4$. The first point to notice is that H_{98y2} varies by about a factor of 2 across the database for each tokamak. This indicates that this reduced description of tokamak energy confinement developed for conventional H mode plasmas is missing at least one variable that plays a significant role in the variation of energy confinement for the advanced inductive plasmas in this dataset. Some trends are apparent in these plots, despite the large variation at any given value of the dimensionless parameters. H_{98y2} increases with ρ_* , decreases with ν^\dagger , and is roughly independent of β_{th} and q_{cyl} .

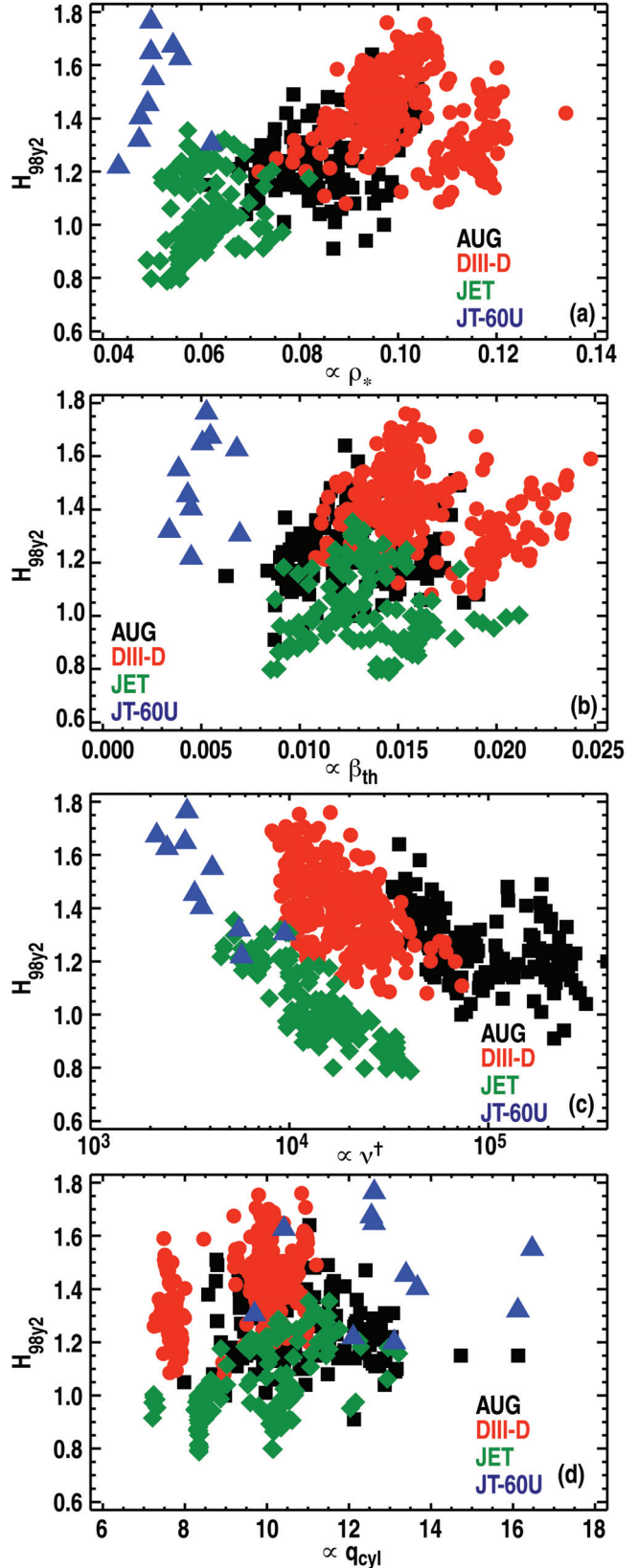


FIG. 4. H_{98y2} vs proxies for dimensionless (a) gyroradius, (b) thermal pressure (ITER range 0.013-0.022), (c) collision frequency, and (d) plasma current as defined in the text. Symbols and colors as defined in Fig. 2.

There is a strong anti-correlation of ρ_* and v^\dagger in this dataset, so it is not possible from this data alone to assign the variation to one or both of these variables, although the JT-60U data breaks this correlation somewhat. The fact that the ITER values of these variables are significantly outside the existing dataset (ρ_* 2x smaller, v^\dagger 10x smaller in ITER) motivates understanding these trends. The variation in H_{98y2} is consistent with a weaker scaling with ρ_* than the gyroBohm scaling ($B\tau_E \propto \rho_*^{-3}$) implicit in H_{98y2} , such as Bohm scaling ($B\tau_E \propto \rho_*^{-2}$). (See Ref. [15] for a general discussion of dimensionless parameter scaling and the definitions and implications of Bohm and gyroBohm scaling.) The trend for H_{98y2} to increase with reduced v^\dagger is also consistent with improved confinement with $T_i > T_e$ and increased rotation associated with the uni-directional neutral beam heating that dominates this dataset. The JT-60U data makes rotation less likely as the cause of the variation, due to lower rotation from more balanced neutral beam injection geometry. The trend is also consistent with the actual scaling being independent of v^\dagger as seen in dedicated v^\dagger experiments in H mode [15]; however, plots (not shown) of the H_{DS03} scaling [16] based on these H-mode dimensionless scaling experiments still show a clear decrease in confinement quality with v^\dagger . The lack of variation with β_{th} may also be illusory, given that the DIII-D and JET data exhibit a trend if plotted for a specific range in q_{95} . It is important to recall that it is not the actual τ_E that is being plotted here; therefore, the trends may reflect dependencies in the data or weaknesses in the scaling used to normalize the data onto a common plot.

Dedicated experiments are needed to clarify these issues; some of these have already been carried out. To clarify the scaling with ρ_* , joint experiments between DIII-D and JET were carried out, including an identity match [17]. It was possible to find matching profiles at the identity point, indicating that the two machines are operating in a common regime. The measured global scaling is close to Bohm scaling, and preliminary analysis of the local transport scaling is also closer to Bohm scaling than to the gyroBohm scaling typical of H-mode plasmas. This is consistent with the trend in H_{98y2} seen in Fig. 4(a). Experiments on DIII-D taking advantage of the ability to vary the applied torque at constant β show a clear improvement in confinement with increasing rotation [18]. Experiments with electron heating (ICRH and ECH on AUG [11] and ECH on DIII-D [19]) show a clear improvement of confinement when $T_i > T_e$, but the effect is weaker than that of rotation, which must be taken into account in these experiments also, because these heating schemes also add no torque. This result is consistent with earlier observations of a weak dependence of confinement in density scans, where T_i/T_e is expected to approach 1 as the density increases. Quantifying these effects is important, since α heating will be dominantly electron heating and provide no torque input.

Figure 5 shows that performance sufficient for $Q > 5$ in ITER has been obtained across a variety of conditions. For ITER, $G=0.3$ should be sufficient for $Q=5$, while $G=0.4$ should yield $Q=10$. As expected, G increases significantly with increasing β_{th} and decreasing q_{cyl} . Good performance has been obtained across broad ranges of ρ_* and v^\dagger . It is interesting that the strong trends of H_{98y2} with v^\dagger do not lead to a similar trend in G .

Modeling activities in the IOS group have focused on the use of transport models to assess the performance in ITER. Various codes have been compared on an ITER reference case under conditions expected for advanced inductive scenarios in order to benchmark the heating and current drive sources (including α particles) and the transport model implementations [20]. Space prevents a complete summary of this activity and only a few key results can be reported here. The simulations with models based on drift-wave theory or 0-D scalings have been compared to existing scenarios using measured profiles and also used to project to ITER performance [21]. As in the baseline scenario, the assumption about the pedestal height is critical to the performance projection. The role of rotation is important for some models

(such as GLF23) [18], while it plays a weaker role in other models (such as the Weiland model) [12]. Recent studies have shown that the GLF23 model is sensitive to the shape of the q profile and suggest that the radial average of s/q , where s is the magnetic shear, may be a key parameter for energy confinement [23]. None of these models has been conclusively shown to model well the whole range of present-day experiments; therefore, the modeling should be viewed as playing a role in suggesting further experiments and indicating the sensitivity of the ITER projections to the various assumptions required, rather than a definitive prediction of ITER performance.

A method to map the allowed operational space including the constraints of the density limit, maintaining H mode, and flux consumption has been developed [24]. Figure 6 shows such a diagram for

long-pulse advanced inductive operation. Specifying goals of 3000 s operation at $Q=5$ with 50 MW of auxiliary heating power, this method indicates that both operating below the density limit and keeping the loss power higher than the L-H threshold power at the operational point requires $I > 10.5$ MA (shaded region of the plot). The values of β_N are in the range of 2.1–2.5, and the confinement implied is a modest improvement over that given by the H-mode scaling. This analysis indicates that the plasma performance required for advanced inductive operation with $P_{\text{fus}} = 250$ MW approaching 1 hour in duration in ITER is within the present physics basis.

Various machines have carried out experiments that exploit their unique capabilities to broaden the physics basis for advanced inductive scenarios. Figure 1 shows an example from JT-60U using the long-pulse capabilities to demonstrate that the current profile reaches stationary conditions at high performance. AUG and DIII-D have carried out joint experiments on pedestal behavior [25]. The two main conclusions are that the pedestal continues to rise as more power flows out through the edge (contrary to some predictions) and that shape changes can have a significant impact on the pedestal parameters. As noted above, the pedestal height plays a significant role in the predictions of ITER performance.

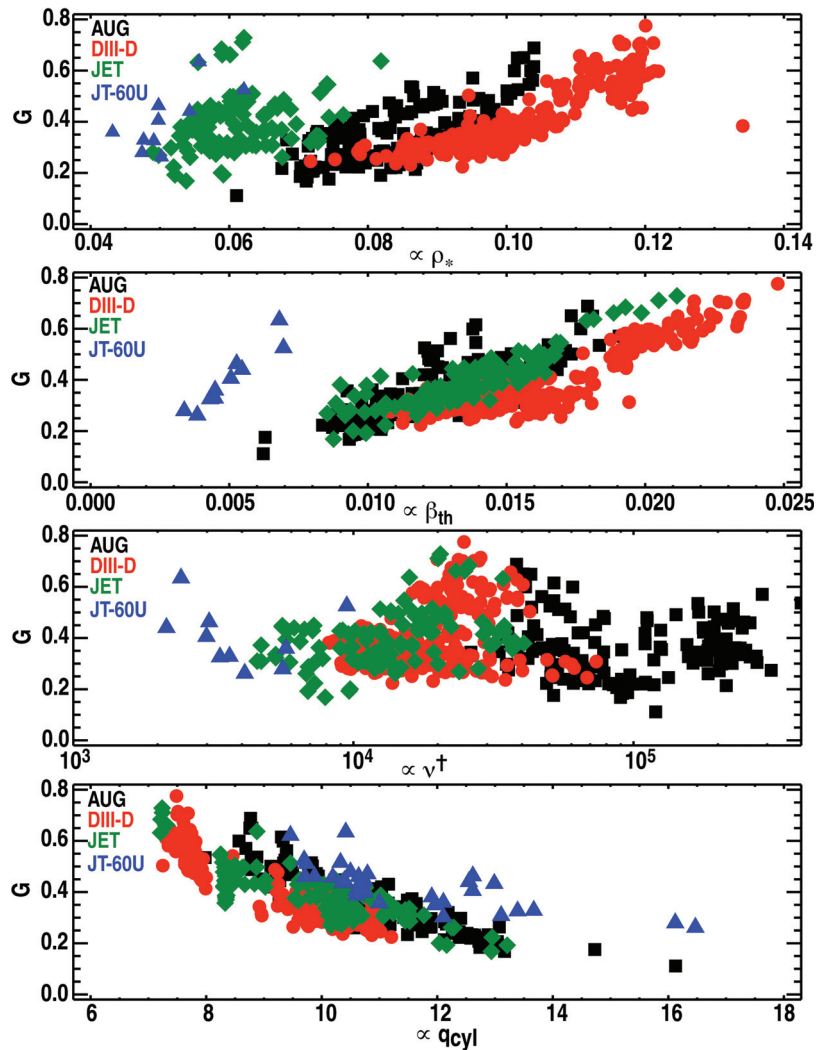


FIG. 5. G vs proxies for dimensionless (a) gyroradius, (b) thermal pressure, (c) collision frequency, and (d) plasma current as defined in the text. Symbols and colors as defined in Fig. 2.

DIII-D has also extended the study of ELM mitigation using non-axisymmetric magnetic perturbations to advanced inductive scenarios [26]. In addition to the joint ρ_* scaling experiments with DIII-D, JET has extended the physics basis for operation at high f_{DL} and for radiative divertor operation to lower ρ_* [27].

It has been suggested that the shape of the current profile could be the origin of both the improved confinement (and perhaps the variation in H_{98y2} seen in the dataset) and the improved stability to $n=1$ tearing modes [20,28,29]. Modeling on AUG [22] and DIII-D [30] indicated the stationary current profile obtained after many τ_R is not consistent with that expected from applying the neoclassical Ohm's law and the standard models for the noninductive external current drive sources. The resulting profile is less peaked, consistent with the small or non-existent sawteeth that are related to a $q=1$ surface in the plasma. In contrast, modeling of JET plasmas [8] appears consistent with expectations of the standard theory. It is plausible to expect enhanced confinement to accompany a flatter q profile, since lower transport from drift waves is predicted [31]. That the current profile should have an effect on tearing mode stability is also plausible, but the theory of tearing stability in high- β toroidal plasmas is not validated sufficiently to provide an optimization strategy for the current profile. Two experiments on DIII-D, alternately suppressing or enhancing the $n=2$ tearing mode amplitude with ECCD [32] and measuring the impact of ELMs on the central current profile through the $n=2$ tearing mode [33] indicate that this mode plays a key role in the current profile evolution beyond a simple modification of the resistivity profile. Fishbones are seen to play a similar role in AUG plasmas [34]. Therefore, MHD modes play both a desirable role (avoiding $q=1$) and an undesirable role (reducing confinement, limiting pressure) in these plasmas.

4. Conclusions

The data collected by the IOS group indicates that these advanced inductive scenarios are a robust mode of operation in divertor tokamaks. The distinguishing characteristics of this mode of operation are stationary operation on the time scale of a fully-relaxed current profile at higher β_N than obtained in conventional H mode operation at low q_{95} , while maintaining good confinement quality. This mode of operation promises to fulfill the high fluence goals of the ITER project, but may also provide a lower-risk alternative approach to achieving the primary physics objective of $Q=10$ operation at 500 MW fusion power for 400 s. While many physics issues surrounding the estimation of performance in ITER are in common with conventional H mode operation (transport, pedestal behavior, radiative divertor operation, ELM mitigation), the current profile evolution and the connection with MHD modes appears to be a distinctive feature of these plasmas. Just as the H-mode pedestal allows the plasma to access a new region of what appears to be a continuum of energy transport behavior, this modification of the stationary current profile may lead to new energy transport behavior by

Hybrid $\Delta t = 3000$ s: $P_{NB} = 33$ MW, $P_{EC} = 17$ MW
Operational limits at $Q = 5$: $P_{loss}/P_{L-H} > 1$, $I_p < 15$ MA

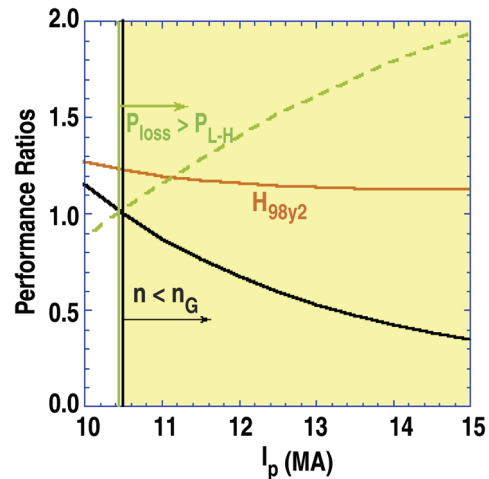


Fig. 6. ITER operational space diagram for advanced inductive operation. The black curve is the ratio of the density to the density limit, the green curve is the ratio of the loss power to the predicted L-H threshold power, and the red curve is the confinement quality measured by the IPB98yw scaling.

accessing current profiles with improved stability to the $n=1$ tearing mode, albeit without an analogous threshold behavior to the H-mode transition. Prescriptions for reaching advanced inductive performance exist for each of the tokamaks represented here; however, access conditions that are necessary and sufficient to reach this regime in ITER have yet to be defined. This remains a high priority task for the IOS group in the near future.

This work was supported in part by the US Department of Energy under DE-FC02-04ER54698, DE-AC02-09CH11466, DE-AC05-00OR22725, and DE-AC05-06ER23100 and by EURATOM within the framework of the European Fusion Development Agreement. The authors gratefully acknowledge the contributions of the ASDEX Upgrade team, the DIII-D team, the JET EFDA Contributors (see the Appendix of F. Romanelli et al., paper OV/1-3, this conference), and the JT-60U team without whom this work would not be possible.

References

- [1] GORMEZANO, C., *et al.*, Nucl. Fusion **47** (2007) S285
- [2] TROYON, F., *et al.*, Plasma Phys. Control. Fusion **26** (1984) 209
- [3] ITER Physics Basis, Nucl. Fusion **39** (1999) 2175
- [4] GREENWALD, M., Plasma Phys. Control. Fusion **44** (2002) R27
- [5] YUSHMANOV, P.N., *et al.*, Nucl. Fusion **30** (1990) 1999
- [6] SIPS, A.C.C., *et al.*, Plasma Phys. Control. Fusion **44** (2002) B69
- [7] LUCE, T.C. *et al.*, Phys. Plasmas **11** (2004) 2627
- [8] JOFFRIN, E., *et al.*, Nucl. Fusion **45** (2005) 626
- [9] OYAMA, N., *et al.*, Nucl. Fusion **49** (2009) 065026
- [10] GRUBER, O., *et al.*, Nucl. Fusion **49** (2009) 115014
- [11] STAEBLER, A., *et al.*, Nucl. Fusion **45** (2005) 617
- [12] MAGET, P., *et al.*, Nucl. Fusion **50** (2010) 045004
- [13] KAMADA, Y., *et al.*, Nucl. Fusion **39** (1999) 1845
- [14] LUCE, T.C., *et al.*, Nucl. Fusion **43** (2003) 321
- [15] LUCE, T.C., *et al.*, Plasma Phys. Control. Fusion **50** (2008) 043001
- [16] PETTY, C.C., *et al.*, Fusion Sci. Technol. **43** (2003) 1
- [17] POLITZER, P.A., *et al.*, this conference, EXC/P2-06
- [18] POLITZER, P.A., *et al.*, Nucl. Fusion **48** (2008) 075001
- [19] PETTY, C.C., Proc. 22nd IAEA Fusion Energy Conference, Geneva, 2008, paper EX1-4rb, http://www-naweb.iaea.org/napc/physics/FEC/FEC2008/papers/ex_1-4rb.pdf
- [20] KESSEL, C.E., *et al.*, Nucl. Fusion **47** (2007) 1274
- [21] IMBEAUX, F., *et al.*, Plasma Phys. Control. Fusion **47** (2005) B179
- [22] NA, YONG-SU, *et al.*, Nucl. Fusion **46** (2006) 232
- [23] CITRIN, J., *et al.*, accepted for publication Nucl. Fusion (2010)
- [24] POLEVOI, A.R., *et al.*, Proc. of 37th EPS Conf. on Plasma Physics, Dublin, Ireland (EPS, 2010) P2.187.
- [25] MAGGI, C., *et al.*, Nucl. Fusion **47** (2007) 535
- [26] HUDSON, B., *et al.*, Nucl. Fusion **50** (2010) 045006
- [27] CORRE, Y., *et al.*, Plasma Phys. Control. Fusion **50** (2008) 115012
- [28] STOBBER, J., *et al.*, Nucl. Fusion **47** (2007) 728
- [29] JOFFRIN, E., *et al.*, Proc. of 22nd IAEA Fusion Energy Conf., Geneva, 2008, paper EX1-4Ra, http://www-naweb.iaea.org/napc/physics/FEC/FEC2008/papers/ex_1-4ra.pdf
- [30] CASPER, T.A., *et al.*, Nucl. Fusion **47** (2007) 825
- [31] WALTZ, R.E., *et al.*, Phys. Plasmas **2** (1995) 2408
- [32] WADE, M.R., *et al.*, Nucl. Fusion **45** (2005) 407
- [33] PETTY, C.C., *et al.*, Phys. Rev. Lett. **102** (2009) 045005
- [34] GUENTER, S., *et al.*, Nucl. Fusion **39** (1999) 1535